CERN – EUROPEAN ORGANIZATION FOR NUCLEAR RESEARCH

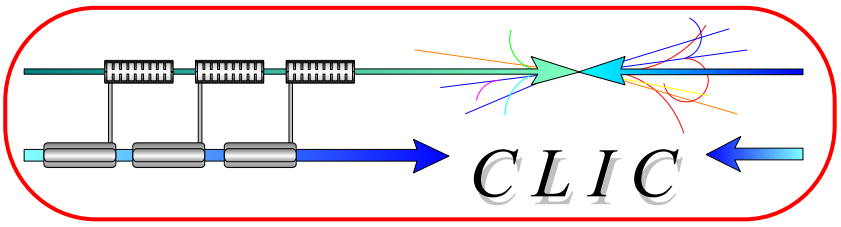

CLIC Note 645

OPTICALLY CONTROLLED 30 GHZ HIGH POWER ACTIVE RF PHASE SWITCH FOR THE CTF3 RF PULSE COMPRESSOR

I. Syratchev, CERN, Geneva, Switzerland
and
G. Denisov, Vl. Kocharovsky, S. Kuzukov, A. Stepanov, IAP, Nizhniy Novgorod, Russia

Abstract

To achieve the high peak power level of 150 MW, necessary to demonstrate the full performance of the new CLIC accelerating structure, a 70 ns RF pulse compressor with resonant delay lines has been built and installed in the CTF3 test area. An active high power RF phase switch would make the operation of the whole 30 GHz power production complex more reliable and robust, with the potential to increase the compression efficiency. By itself, such a device can be used for many other applications. In this paper we propose a possible solution based on an over-moded RF circuit with active element made from a semiconductor controlled by a laser beam.

Geneva, Switzerland
15/11/2005

Optically Controlled 30 GHz High Power Active RF Phase Switch for the CTF3 RF Pulse Compressor

I. Syratchev, CERN, Geneva, Switzerland
and
G. Denisov, Vl. Kocharovsky, S. Kuzukov, A. Stepanov, IAP, Nizhniy Novgorod, Russia

Abstract: To achieve the high peak power level of 150 MW, necessary to demonstrate the full performance of the new CLIC accelerating structure, a 70 ns RF pulse compressor with resonant delay lines has been built and installed in the CTF3 test area. An active high power RF phase switch would make the operation of the whole 30 GHz power production complex more reliable and robust, with the potential to increase the compression efficiency. By itself, such a device can be used for many other applications. In this paper we propose a possible solution based on an over-moded RF circuit with active element made from a semiconductor controlled by a laser beam.

1. Introduction.

The recent progress in the CLIC accelerating structure design makes challenging demands on the 30 GHz RF pulsed power production. Over 150 MW during 70 ns are required to demonstrate the full performance of the new CLIC accelerating structure HDS [1]. To this end, a dedicated beam line, special power generating structure and power transfer line with reduced losses have been designed, installed and commissioned in CTF3 (CLIC Test Facility). In 2004, 52 MW during 74 ns were delivered to the high gradient test area [2]. This peak power level is well below the new target value. A 70 ns pulse compressor with resonant delay lines [3,4] has been designed and manufactured in GYCOM [5]. It has been installed in a high gradient test area to provide higher peak power. The pulse compressor consists of two identical, 9 m long delay lines, made of 50 mm diameter circular waveguides, operating at a low loss H_{01} mode. Each line is equipped with 2 vacuum pumping ports, movable short circuit, waveguide taper and mode converter. The general view of the pulse compressor is shown in Fig. 1. The system has been tested at low RF power. The round trip RF power losses of 1.8 % are in agreement with the expected value. The examples of the pulse envelopes reconstructed from these measurements are shown in Fig. 2.

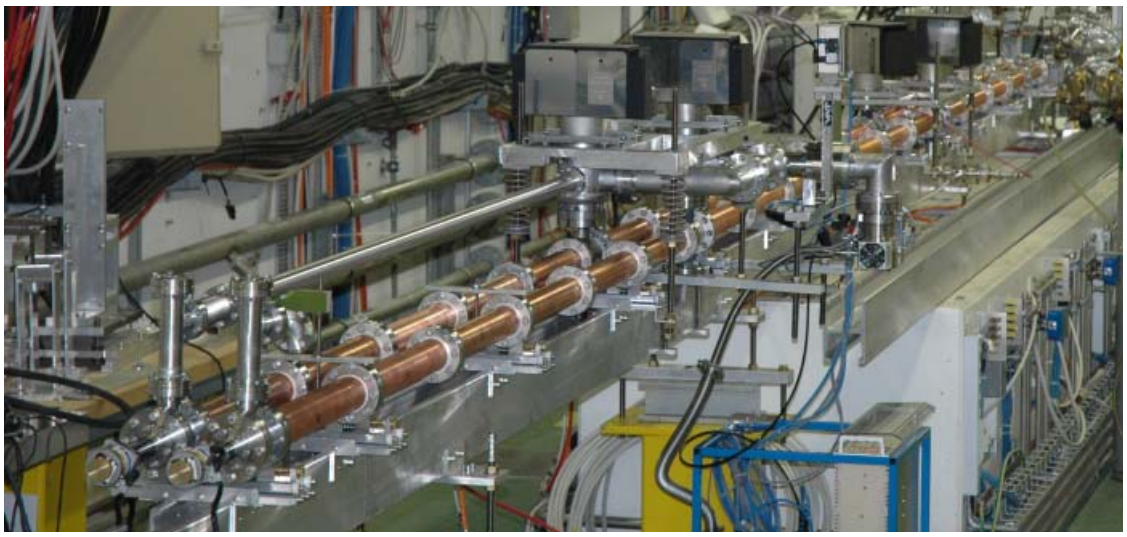

Figure 1. General layout for the 30 GHz pulse compressor in the high gradient test area.

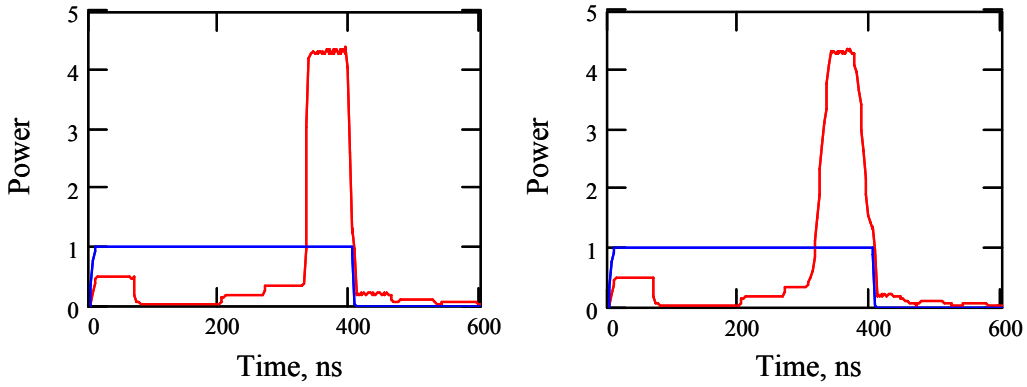

Figure 2. The pulse envelopes reconstructed from the single delay line low power measured spectrum for the two different switching times, 10 ns (left) and 50 ns (right).

To make the pulse compressor system operate efficiently, a fast 180° RF phase flip should be provided. At present it is foreseen to achieve this by switching the CTF3 3 GHz drive beam phase by 18°, which translates into the required 180° at 30 GHz [6]. Dedicated high power tests are planned for early 2006. However, this method will remain complicated due to the fact that the speed of the RF phase switching will be limited by the 3 GHz system, in particular by the filling time of the CTF3 accelerating structures. These effects can adversely affect the shape of the compressed pulse reducing the flat top duration, see Fig. 2 for example. A system capable of handling tens of MW at 30 GHz and providing a fast (few ns) electronically controlled rf phase flip would be much easier to operate. High power, high frequency active switches have been proposed and evaluated for more than 10 years, see [7-10] for example. Unfortunately, none of them have yet demonstrated the capability to work at the power levels we are aiming at. Also, these devices were designed to manipulate both RF pulse phase and amplitude.

In general, to make RF phase manipulations at constant amplitude, 4-port or 2-port RF circuits can be used. For example, one can think of a standard 3 dB hybrid where 2 ports have short circuits, the positions of which can be electronically controlled. Another approach is to directly control the phase delay (in this case the length) in 2-port devices. In this paper we present a 2-port device as a possible solution for the high power active RF phase switch, which is based on over-moded components developed by GYCOM for CTF3.

2. An optically Controlled 30 GHz High Power Active RF Phase Switch.

The description of the device can be split into two parts: the RF circuit configuration and the method of active control at a high power level. For the second part, we are considering to use a solution similar to the one proposed and basically demonstrated in [7], where a short laser pulse of a certain wavelength converts the surface layer of a silicon wafer into the conducting state so that RF power can be efficiently reflected. The detailed description of the underlying process is discussed elsewhere [7, 11-12]. For the RF circuit, we suggest the use of an over-moded 90° mitre bend [5]. Three such devices were installed and successfully operated at high power in the CTF3 transfer line (see Fig. 3). In this device, the following mode mixing technique is used: initially, along the waveguide taper, the incident H_{01} mode is converted to a mixture of the three modes – H_{01}, H_{02} and H_{03}. The amplitudes and phases of these three modes are specially adjusted such that at a certain distance the RF wave is focused to a waist. A 45° copper mirror is placed at this position deflecting the RF power towards the output waveguide, where the reconstruction of the original H_{01} mode occurs. The plot of the instant electric field amplitude simulated by HFSS is shown in Fig. 3.

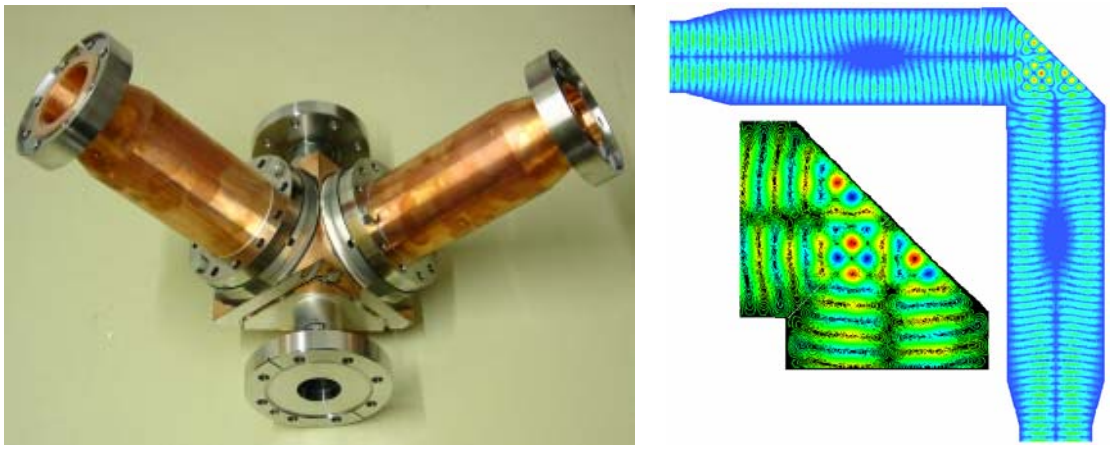

Figure 3. General view of the 90° overmoded mitre bend and the instant electric field distribution at the median plane of the bend as simulated by HFSS.

The principle of operation of the active RF phase switch is illustrated in Fig. 4. The thin silicon wafer is attached to the copper mirror providing good thermal contact. The incident RF power goes through the wafer, resulting in a certain RF phase advance due to reflection at the backplane of the wafer. At the required moment, a short laser pulse (few nanoseconds) irradiates the semiconductor surface and converts it into the conducting state, such that RF power is reflected at the wafer's front plane, resulting in a fast 180° RF phase flip.

Compared to other proposed schemes [7-10], this scheme provides certain advantages: due to the large surface area, the surface electric field strength will be significantly reduced; this allows for high power capability. The absence of field at the periphery of the mirror makes it easy to install and leaves enough space to introduce the laser beam and vacuum pump feed-throughs. The direct thermal contact of the wafer to the copper mirror will reduce the overall heating of the silicon wafer during operation.

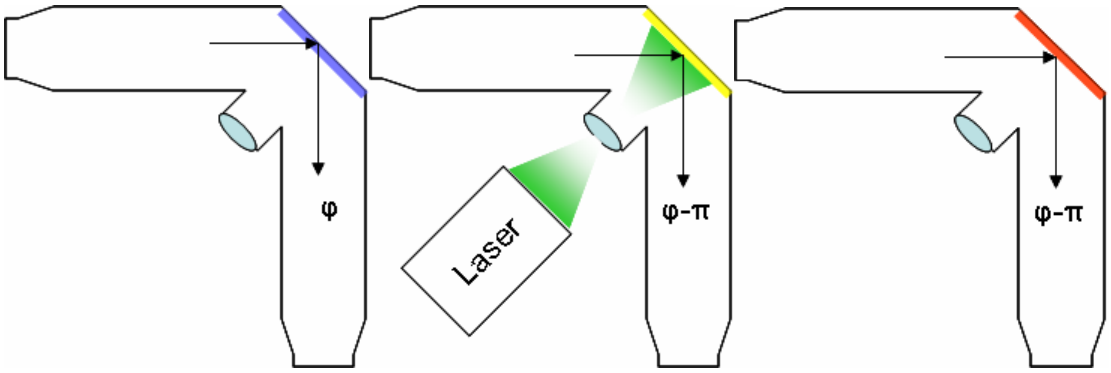

Figure 4. The three stages of operation of the high power optically controlled active rf phase switch.

The thickness of the semiconductor should be chosen such that the phase advance between the active state and passive states of the switch will be 180°. Thus the dielectric properties of the material must be taken into account. We made the following initial analytical analysis to understand this requirement.

First we consider that at the mirror surface the prepared mode mixture behaves as a paraxial wave beam. In this approximation we can use a plane (two dimensional) model, when the incident wave is reflected from the perfect mirror with the dielectric layer on it. However, because of its nature, the incident wave will have two polarizations with respect to the mirror surface. In one case, $E_y \neq 0$, but all the other components of the electric field are equal to zero (*E*-polarization), in the other case, $H_y \neq 0$, and all the other magnetic field components are equal to zero (*H*-polarization). We study three configurations following the RF phase shifter states of operation, see Fig. 5. (1): perfect mirror at $x = 0$, (2): dielectric layer (representing the Si wafer) of thickness l placed on the perfect mirror, and (3): perfect mirror at $x = l$.

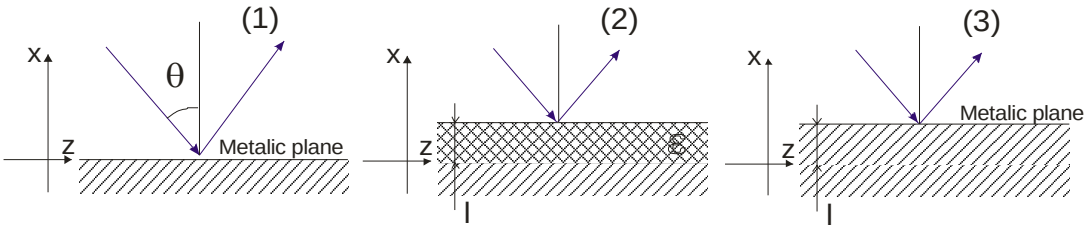

Figure 5. The three configurations for analysis, following the RF phase shifter states of operation.

For configuration (2), the complex reflection coefficients for the two polarizations can be written as:

$$R_E^{(2)} = e^{-i2k_1 l + i\pi} \cdot \frac{k_2 \cdot \cos(k_2 l) + ik_1 \cdot \sin(k_2 l)}{k_2 \cdot \cos(k_2 l) - ik_1 \cdot \sin(k_2 l)} \tag{1}$$

for the *E*-polarization, and

$$R_H^{(2)} = e^{-i2k_1 l} \cdot \frac{k_1 \cdot \cos(k_2 l) + ik_2 \cdot \sin(k_2 l)}{k_1 \cdot \cos(k_2 l) - ik_2 \cdot \sin(k_2 l)} \tag{2}$$

for the *H*-polarization. Here $k_1 = k \cdot \cos\theta$, $k_2 = k \cdot \sqrt{\varepsilon - \sin^2\theta}$,and $k = \omega/c$. In general, the complex phases of $R_E^{(2)}$ and $R_H^{(2)}$ are different, and they are periodical functions of the thickness *l*. We are looking for the special solution where the phase difference between the configuration (2) and (3), $\arg\left(R^{(**)}\right) = \arg\left(R^{(2)}\right) - \arg\left(R^{(3)}\right)$ is 180°. We also consider $\arg\left(R^{(*)}\right) = \arg\left(R^{(2)}\right) - \arg\left(R^{(1)}\right)$, the phase difference between configuration (1) and (2). Using equations (1) and (2) together with the conditions $\arg\left(R_E^{(1)}\right) = \pi$, $\arg\left(R_E^{(3)}\right) = \pi - 2kl\cos\theta$, $\arg\left(R_H^{(1)}\right) = 0$ and $\arg\left(R_H^{(3)}\right) = -2kl\cos\theta$, we get the optimal thickness of the layer when $\arg\left(R_E^{(**)}\right) = \pi$:

$$l_{opt} = \frac{\pi}{2k_2} = \frac{\lambda}{4\sqrt{\varepsilon - \sin^2\theta}}, \tag{3}$$

where λ is a wavelength. This is true for both polarizations, because the dielectric layer of this specified thickness is resonant at a given frequency and the phase of reflection in this case does not depend on the polarization. Another important result is that for this optimal thickness, the condition $\arg\left(R_E^{(*)}\right) = \arg\left(R_H^{(*)}\right)$ is also satisfied. This means that there are no extra losses due to polarization distortions in the passive state of the switch because the transverse structure of the field for the reflected wave beam is not perturbed with respect to the structure of the incident wave beam. The relative phase of reflections $\arg\left(R^{(**)}\right)$ and $\arg\left(R^{(*)}\right)$ versus dielectric layer thickness for the two polarizations and the optimal thickness as a function of the relative permittivity of the layer material are shown in Fig. 6.

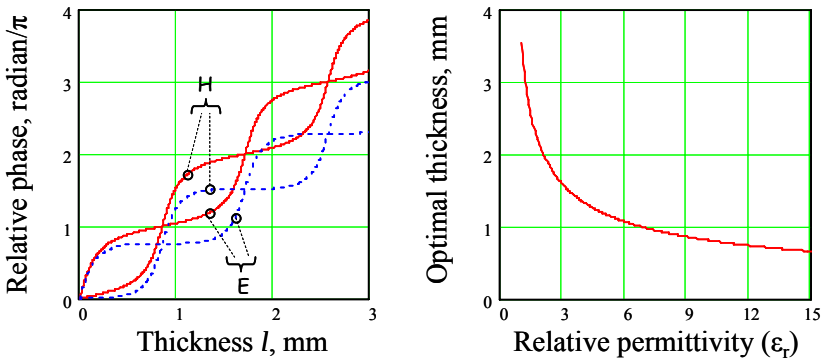

Figure 6. Left: relative phases of reflection for the two polarizations: $\arg\left(R^{(**)}\right)$ (solid lines) and $\arg\left(R^{(*)}\right)$ (dashed lines). Right: optimal dielectric thickness as a function of the relative permittivity of the layer material.

Subsequently we have made full HFSS simulations for the two states of the switch. An optimum thickness of the wafer was chosen according to our analytical results. The copper mirror was shifted by half of the wafer thickness from its original position. 25 port modes were used in the

simulations. The need to simulate half of the full geometry and a large object size-to-wavelength ratio led to the huge amount of simulations. However, the convergence of the solutions was not satisfactory and the conclusions presented below should be considered rather preliminary. Nevertheless, the electric and magnetic field amplitudes, as well as matrix data and post processing represent rather reliable results.

The first group of results is shown in Fig. 7. Here the real part of the instant amplitude of the electric field at the switch median plane is shown for both cases. Input port (upper on the picture) is excited with the proper mode mixture. At the output port, one can see the changes in colors from one state to another, which indicates 180° phase difference between the two states. Fig.7 also shows the phase of the normal component of magnetic field along the line from the center of the wafer surface to the output port. Again, a total phase flip of 180° is clearly visible. Thus we may conclude that, within the assumptions made, the switch will function as expected.

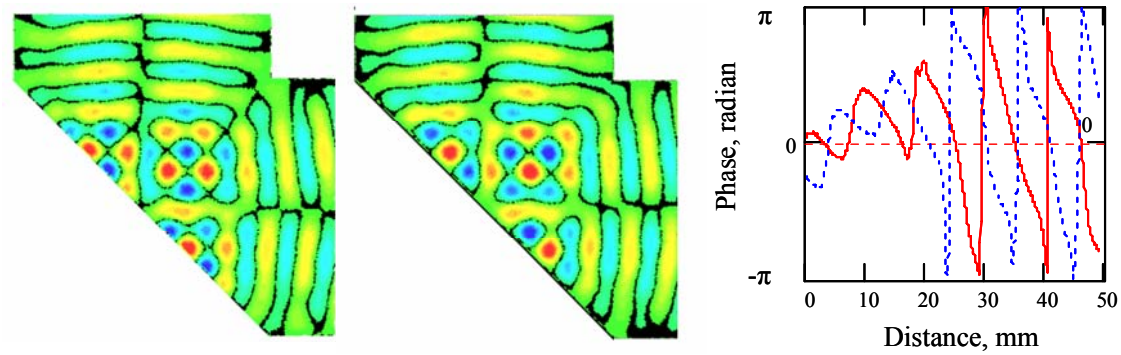

Figure 7. The Electric field plots on the bend median plane in the passive state (left) and in the active state (right), calculated with HFSS. The phase of the magnetic field normal component along the line from the wafer surface to the center of the output port.

Fig. 8 shows the complex magnitudes of the surface electric field at the silicon wafer surface for both cases. In the passive state the electric surface field is almost tangential and its maximum amplitude is 1.8 kV/m for 1 W of input power. The normal component of the electric field from the copper mirror side in this case is 0.46 kV/m. In the active state the field is normal to the surface and its maximum amplitude is 1.35 kV/m for 1 W of the input power.

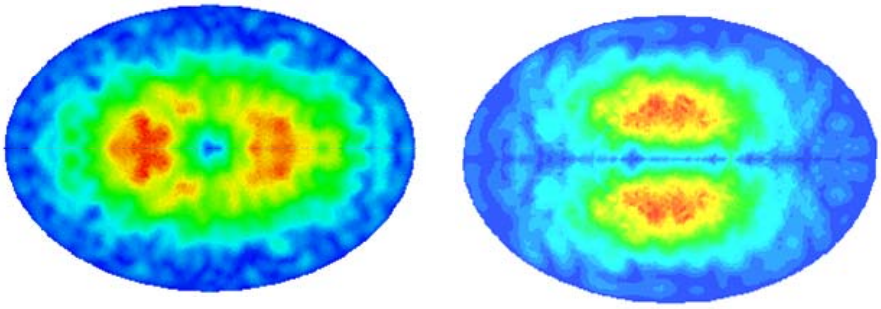

Figure 8. The electric field plots on the surface of the silicon wafer for the passive (left) and active (right) state as simulated by HFSS.

To avoid surface breakdown or flashover during high power operation, the silicon wafer should not be exposed to an electric field that exceeds a certain limit in the passive state. Different values for this threshold field can be found in the literature. For our estimates we use the electric field limit of 10 MV/m, as suggested in [7]. This limit results in a power limit of 32 MW of the system. To achieve 150 MW in a compressed pulse would require a power compression by a factor 5, and consequently 500 ns long input pulses based on the measured performance of the pulse compressor. These parameters – 32 MW during 500 ns – agree well with the available capacity of the 30 GHz RF power source in CTF3.

To minimize losses in the passive state and hence to reduce the thermal heating of the silicon wafer, we need to have a very pure semiconductor material such that the intrinsic carrier density is very small. In the active state, when the plasma layer is excited, the carrier density should be large enough

for the semiconductor to act as a good conductor and thus minimize the losses. At a carrier density of $10^{19}/cm^3$, silicon has a conductivity about 0.6 % that of copper [7]. Thus the skin depth of the material at our frequency is about 5 μm.

We have estimated the losses in the silicon wafer during the passive state using HFSS. For our frequency, a loss tangent of 10^{-3} of the high-resistivity silicon without any doping was assumed; this resulted in overall losses of 0.76 %. Next, we have simulated with ANSYS the pulse temperature rise for the hottest spot in the bulk of the silicon wafer using HFSS data and the RF signal parameters as defined above. In the passive state the pulsed temperature rise of the wafer bulk was about 0.2 K. In the active state, for the expected conductivity of the layer, the surface pulsed temperature rise was 2.3 K. Note that in the active state the hottest spot has a different location to that in the passive state (see Fig. 8). The average heating of the wafer was simulated for a 100 Hz repetition rate and direct water cooling of the copper mirror, see Fig. 9. Assuming 20 °C cooling water, the maximum average temperature of the silicon wafer should be 45 °C. As one can see in Fig. 9, this temperature is dominated by the RF losses in the passive state. The RF losses in the silicon are very sensitive to its temperature. One way to reduce them is to use special doping. In [13] it was shown that the use of gold as doping agent can reduce the loss tangent of the high-resistivity silicon by a factor of more than 10. Thus, with direct cooling of the copper mirror, the problem of silicon wafer heating will be completely solved.

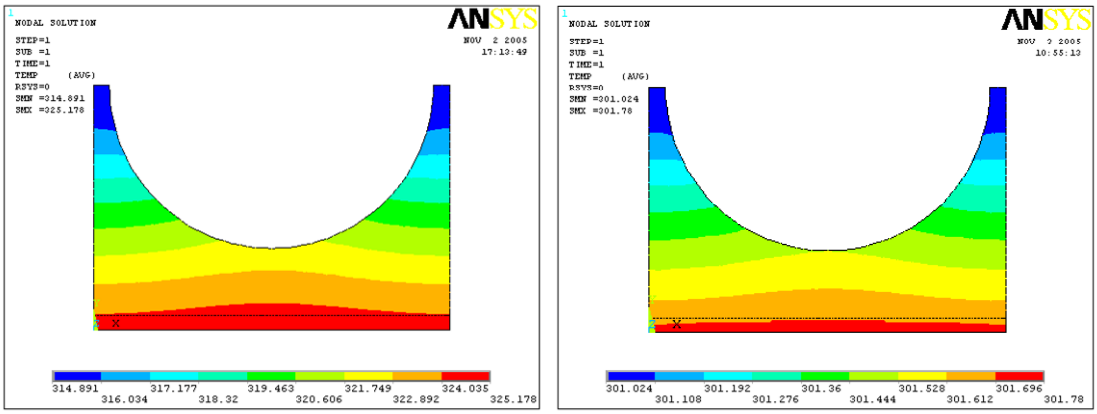

Figure 9. The steady state temperature distribution close to the silicon-copper interface with direct cooling of the copper mirror and a 100 Hz repetition rate. Left on the picture for the passive state, right for the active state.

3. Lower RF power experimental measurements of the silicon wafer reflectivity initiated by laser.

To make efficient use of the laser power, the laser wavelength should be chosen such that the optical absorption depth is comparable to the RF skin depth of the silicon in its conducting state. The dependence of the optical absorption depth as a function of the laser wavelength is shown in Fig. 10 [17].

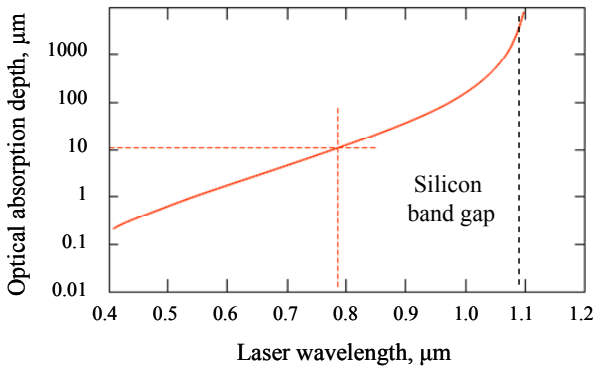

Figure 10. Dependence of the optical absorption depth as a function of the laser wavelength.

A laser system based on a Ti:Sa femtosecond laser with a carrier wavelength $\lambda = 795$ nm was used in this experiment [16]. This wavelength corresponds to the case when the optical absorption

depth is twice the expected RF skin depth at 30 GHz, i.e. 10 μm (see Fig. 10). The laser parameters are: spectrum width ≈ 15 nm, energy in a pulse ≤ 10 mJ, repetition rate 10 Hz. To provide the nanosecond range laser pulses, the regenerative amplifier was used in a system as an oscillator. The ~9 ns laser pulses were measured at the output of a system using a fast photodiode. Tuning of the laser pulse energy was done with a polarized attenuator. At the surface of the silicon wafer, the initial laser beam-spot of approximately 0.2 cm^2 was later defocused by a lens with a negative focal length of 76 mm to about 10 cm^2.

As for the silicon sample, we have used high-resistivity silicon with reduced losses, specially developed at IAP for high power gyrotron windows [14]. The measured 30 GHz silicon parameters are: $\varepsilon_r \approx 11.7$ and $\tan\delta \le 5\cdot 10^{-5}$. The schematic layout and the general view of the test set-up are shown in Fig. 11. The test set-up was calibrated by replacing the silicon with a copper disk. The angle of RF incidence was close to the 45° used in a miter bend, but the operating mode was different: H_{11} instead of H_{01}.

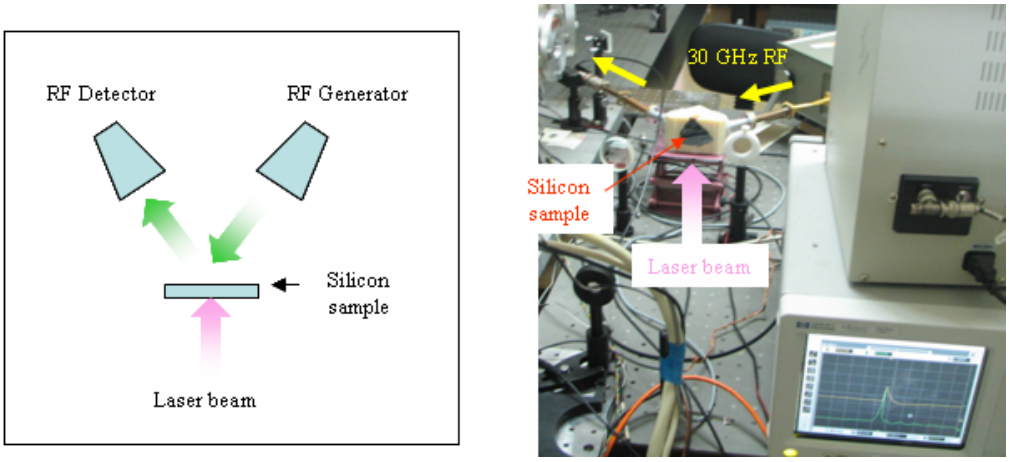

Figure 11. The schematic layout and the general view of the test set up.

A 2.87 mm thick silicon wafer with 9 cm^2 of total surface area was used in the tests. At the operating frequency 30.48 GHz and the chosen angle of incidence, this wafer is fully transparent in its passive state. This allows the best decoupling of the generator and detector during the passive state and the best coupling in the active state. The measured RF reflection from the silicon wafer irradiated by a laser as a function of time is shown in Fig. 12 for the different laser pulse energies.

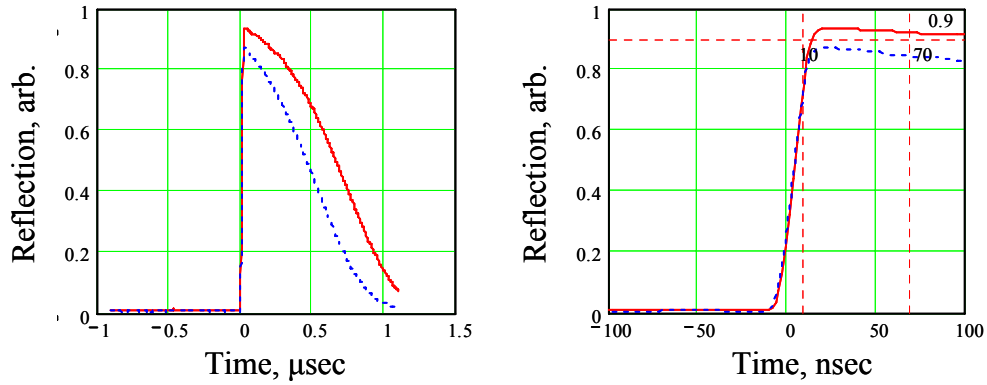

Figure 12. Amplitudes of the reflected power from the silicon wafer before and after the laser pulse. Solid line is for the laser energy 4.4 mJ and dashed line for 2 mJ.

4. Discussion

The experimental results for the laser control of the silicon wafer reflectivity, even made in a very rudimentary environment, have proven that this technique has a good potential for our purposes. We measured fast rise times of about 10 ns. For the highest laser energy, the free carrier life time provided reflection in excess of 90 % for about 100 ns. A total relaxation period of about 1.5 μs was measured for this case. The tests showed that higher laser energy improves the performance. However, much

more should be done to optimize the real optics of the system in order to minimize the demands on the laser energy and thus to reduce the overall cost.

In the near future we plan a series of high power tests to experimentally establish the surface electric field breakdown threshold of the silicon. The 30 GHz FEM at JINR (Dubna, Russia) is currently available and can provide about 20 MW RF power during 200 ns [15].

We conclude after this preliminary study of a 30 GHz high power active phase switch that the pulsed power level of 150 MW required in CTF3 seems well in reach. The mechanical design of the system should be started. Later we suggest dedicated low power tests for the whole device, where the silicon wafer can be replaced by different dielectric or metal discs; these tests can be considered as an experimental proof of principle for the switch operation.

References

1. Grudiev A., Wunsch W.: 'A Newly Designed and Optimized CLIC Main Linac Accelerating Structure', LINAC 2004, Lubeck, Germany, 16 - 20 Aug 2004.
2. Wunsch W., et al.: '30 GHz Power Production in CTF3', PAC 2005, Knoxville, TN, USA , 16 - 20 May 2005.
3. Fiebig A., Schlieblich C.: 'A Radiofrequency Pulse Compressor for the Square Output pulses', EPAC 1988, Rome, Italy, June 1988.
4. Wilson P.B., Farkas Z.D. and Ruth R.D.: 'SLED II: A New Method of RF Pulse Compression', Linac 1990, Albuquerque, NM, USA, September 1990.
5. Kuzikov S.: '30 GHz Power Line and SLED-II Pulse Compressor for CTF3 ', Minutes of the CLIC Meeting, 6 August 2004, CERN, Geneva, Switzerland, 2004.
6. Braun H.: 'Beam line/commissioning' Minutes of the Ninth CLIC/CTF3 Collaboration Meeting, CERN, Geneva, Switzerland, November 2004.
7. Tantawi S. G., Ruth R. D. and Vlieks A. E.: 'Active High-Power RF Pulse Compression Using Optically Switched Resonant Delay Lines', 7th Workshop on Advanced Accelerator Concepts, Lake Tahoe, CA, USA, October 1996
8. Vikharev A.: 'Plasma Switch for X-band Active SLED II Pulse Compressor', 11th Workshop on Advanced Accelerator Concepts, Stony Brook, NY, USA, June 2004.
9. Tamura F., Tantawi S. G.: 'Development of High Power X-band Semiconductor RF Switch for Pulse Compression System of Future Linear Collider', Linac 2000, Monterey, CA, USA, August 2000.
10. Tantawi S.G.: 'Overmoded High Power Magnetic Switches and Circulators', PAC 2001, Chicago, IL, USA, June 2001.
11. 'Optoelectronic Switches for Pulsed Power', in Picosecond Optoelectronic Devices, Chi H. Lee, Editor, Academic Press, pp. 374-398, Orlando, Florida, 1984.
12. Nunnally W. and Hammond R.: 'Photoconductive Power Switches', Los Alamos National Laboratory Report, LA-9759-MS, April 1993.
13. Parshin V. et al.: 'Silicon as an Advanced Window Material for High Power Gyrotrons', Int. J. Infrared Millimeter Waves, vol. 16, pp. 863-877, 1995.
14. Parshin V. et al.: 'Silicon with Extra low Losses for Megawatt Output gyrotron windows', 20th International Conference on Infrared and Millimeter waves, Orlando, USA, M2.4, 1995.
15. Peskov N. et al.: "Repetitive 30-GHz free electron maser applicable for RF testing properties of materials", 15th Int. Conf. on High-Power Particle Beams (BEAMS'2004), St. Petersburg, Russia, July 18-23, 2004, p.438-441.
16. A. P. Aleksandrov, A. A. Babin, A. M. Kiselev, D. I. Kulagin, V. V. Lozhkarev and A. N. Stepanov: "Terawatt femtosecond Ti:Sa laser complex", Quantum Electronics, **31,** 398-400 (2001).
17. Nunnally W. and Cooperstock D.: 'Methods and Configurations for Improving Photo-Conductive Switch Performance', 25th International Power Modulator Symposium 2002 and 2002 High-Voltage Workshop, 2002, pp. 183-186.